Modelling Particle Tracking of Moisture Droplets in Geothermal Steam Pipeline

Kim Fong Chan* and Sadiq J. Zarrouk

Department of Engineering Sciences, The University of Auckland, Private Bag 92019, Auckland, New Zealand

*kcha736@aucklanduni.ac.nz

Keywords: *Steam quality, steam purity, water droplets, entrainment, deposition, system above ground, water wash, SPDOT.*

ABSTRACT

As the saying goes, "A persistent drop of water will wear away the hardest stone", very small water droplets in micro-scale in the steam can damage the turbine over time. Many studies on the steam quality found that although it is within the turbine manufacturer's limit and has 99.95% of dryness and above, the turbine still suffers from water impingement erosion and mineral scaling. The basis of water carryover from the separator and condensation in the steam line is adapted from the Steamfield Process Design and Optimisation Tool (SPDOT) by Umanzor & Zarrouk (2022). This work presents a comprehensive carryover analysis, water droplets interactions, and entrainment rate. This is to provide a better understanding of the system's moisture droplets and current equipment's limitations in capturing these water particles before entering the turbine.

1. INTRODUCTION

1.1 Geothermal power plants

New Zealand's first geothermal power plant in Wairakei has been long-standing since it was commissioned in 1958. One of the key successes of this plant to this date can be attributed to its cross-country pipeline up to several kilometres that allow for sufficient steam scrubbing to attain high quality and purity of steam arriving at the turbine's inlet.

More recent power plants are designed and built in more compact environments, with the separation plant close to the power plant. The short distance reduces the overall costs of a project as the pipelines can be built faster, and smaller diameter pipelines can be used as pressure drop will not be a concern. Zarrouk & Purnanto (2015) recommended a minimum of 400 meters length of pipeline to allow for sufficient scrubbing.

Turbine problems such as erosion and mineral deposition started to arise as the newer power plants start operating. A few cases have been reported by Morris et al. (2019); Morris & Mroczek, (2015); Richardson et al. (2013) and many more cases were believed to be not reported. When the turbine is damaged, the power plant would have to shut down for turbine repair, which may take a day or weeks, depending on the damage.

As a baseload power generation, a geothermal power plant should run at the design capacity without a major breakdown. Hence, the turbine's longevity and performance are highly significant. The water particle tracking model is developed to aid in the troubleshooting of the moisture removal system. The model aims to predict the final steam quality entering the turbine by applying entrainment correlations from relevant literature. This will help to diagnose each section of the system and provide insights on which section to improve to get the best steam quality and purity. Steam quality is a measure of the dryness of the steam, while steam purity is a measure of the cleanness of the steam.

1.2 Existing models

Recently, a few models to model steam purity were established mainly the Geothermal Steam Purity (GSP) model by Mills & Lovelock (2020) and the SPDOT by Umanzor & Zarrouk (2022). These models covered the separator efficiency calculations, pipeline heat loss, pressure drop, mineral dilution, Silica distribution coefficient, and mass balance from water wash. These calculations serve as the fundamental of this work.

1.3 Droplets carryover

The Mills & Lovelock (2020) and Umanzor & Zarrouk (2022) models focused on the carryover water as a liquid film flowing at the bottom of the pipe and did not consider the flying droplets that advance together with the steam. However, it has been acknowledged by several researchers that there is water carryover in the form of droplets alongside the water that flows at the bottom of the pipe. This is also known as the two-phase, three-field flow by Bae et al. (2018), as shown in Figure 1.

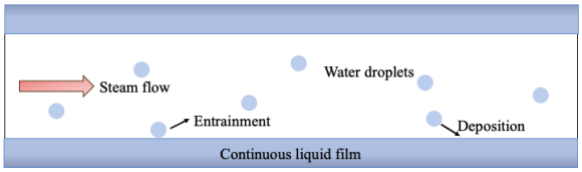

Figure 1: Two-phase, three-field flow in a steam pipeline.

A notable study on water particle tracking in the separator was conducted by (Pointon et al., 2009) through computational fluid dynamics (CFD) simulation. CFD is a beneficial tool to provide insights into the separator's flow to aid in our understanding through visualisation. 8 water droplets of 3µm diameters were injected into two different designs of separator, according to Bangma (1961) and Lazalde-Crabtree (1984). The Lazalde-Crabtree (1984) separator can remove 99.987% of the droplets, while the Bangma (1961) separator cannot do so.

Despite there is availability of CFD study to track water droplets in the separator, there is no CFD study done in the steam pipelines for water droplets entrainment and deposition.

Ishii & Grolmes (1975) developed a criterion to determine the inception of entrainment in the two-phase flow.

$$Re_f = \frac{4\rho_l u_l \delta}{\mu_l} = \frac{4\Gamma}{\nu_l} \quad (1)$$

where,

Proceedings 45th New Zealand Geothermal Workshop
15-17 November, 2023
Auckland, New Zealand
ISSN 2703-4275

Re_f	Reynolds number of liquid film
ρ_l	Density of liquid (kg/m^3)
u_l	The velocity of the liquid film (m/s)
δ	The average thickness of the liquid film (m)
μ_l	Dynamic viscosity of liquid (kg/m·s)
Γ	Volumetric flow rate per unit wetted perimeter (m^2/s)
ν_l	Kinematic viscosity of liquid (m/s)

Shearing off from roll-wave crests happens in the range of 160 to 1635Re_f, also known as the transition regime. While for Re_f more than 1635, entrainment based on the roll-wave mechanism happens (Figure 2).

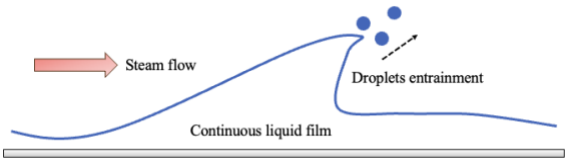

Figure 2: Roll wave entrainment mechanism.

Van Rossum (1959) developed a simpler criterion to predict entrainment, in which no atomisation is possible below the critical gas velocity.

$$u_{v,cr} = 250\sigma \tag{2}$$

where,

$u_{v,cr}$	Critical gas velocity
σ	Surface tension (N/m)

2. ENTRAINMENT CORRELATIONS

Entrainment of the water droplets carried over from the separator and while transporting the steam from the separator to the power plant is an important factor in the steam purity. The amount of entrainment allows for predicting potential turbine damages, but it also informs which part of the moisture removal system should be enhanced when designing a new system or when retrofitting an existing system.

2.1 Entrainment fraction

Entrainment fraction is the ratio of water droplets flow in the gas core to the total liquid flow. The fraction is dimensionless and has values ranging from 0 to 1.

$$E = \frac{m_d}{m_{lt}} = \frac{m_d}{m_d + m_l} \tag{3}$$

where,

E	Entrainment fraction
m_d	Droplet mass flow (kg/s)
m_l	Liquid film mass flow (kg/s)
m_{lt}	Total liquid mass flow (kg/s)

A few different types of correlations were established based on the experimental data of the type of flow used. The correlations can be for vertical or horizontal flow or both.

Ishii & Mishima (1984) developed a straightforward and easy entrainment correlation that applies to both flows.

$$E = \tanh\left(7.25 \times 10^{-7} \times We^{1.25} \times {Re_l}^{0.25}\right) \tag{4}$$

$$We = \frac{\rho_v {j_v}^2 D}{\sigma}\left(\frac{\Delta\rho}{\rho_v}\right)^{1/3} \tag{5}$$

$$Re_l = \frac{\rho_l j_l D}{\mu_l} \tag{6}$$

where,

We	Weber number
Re_l	Liquid Reynolds number
ρ_v	Density of vapour (kg/m^3)
j_v	Superficial velocity of vapour (m/s)
j_l	Superficial velocity of liquid (m/s)
D	Pipe diameter (m)

Sawant et al. (2008) further developed the correlations above into three regions for vertical flow with a modified Weber number.

$$E = E_m \tanh\left(a {We_v}^{1.25}\right) \tag{7}$$

$$E_m = 1 - \frac{Re_{fflim}}{Re_l} \tag{8}$$

$$We_v = \frac{\rho_v {j_v}^2 D}{\sigma}\left(\frac{\Delta\rho}{\rho_v}\right)^{0.25} \tag{9}$$

$$Re_{fflim} = 250 \times \ln(Re_l) - 1265 \tag{10}$$

$$a = 2.31 \times 10^{-4} {Re_l}^{-0.35} \tag{11}$$

where,

We_v	Modified Weber number
Re_{fflim}	Limiting liquid film Reynolds number

Al-Sarkhi et al. (2012) developed a new approach that only requires the superficial velocity of vapour and liquid and is valid for both horizontal and vertical flow.

$$E = E_m\left[1 - exp\left(-\frac{We_v}{We_v^*}\right)\right] \tag{12}$$

$$E_m = E_{lim}\left[1 - exp\left(-\left(\frac{Re_l}{Re_l^*}\right)^{0.6}\right)\right] \tag{13}$$

where,

E_{lim}	Limiting value of the maximum entrainment fraction
We_v^*	Analogous time constant Weber number
Re_l^*	Analogous time constant Reynolds number

The E_{lim} is a little less than 1. Any value of 0.98-1.00 can be used. The Re_l^* has been determined to a value of 1400 at 63.2% of the maximum entrainment fraction when it reaches its limiting value near 1. These values were empirically established using various air-water experimental data in the vertical and horizontal pipe. Graph of E vs We_v^* has to be plotted to obtain the value of We_v^* at $E = 0.632E_m$.

Lee et al. (2022) developed two models for horizontal flow in a higher pressurised system up to 70 bar. In this work, only model 2 is discussed as it has better predictability and a lesser error percentage. This model involved a modified dimensionless film thickness from Mantilla (2008) with a combination of Pan & Hanratty (2002) entrainment model.

$$\frac{(E/E_m)}{1-(E/E_m)} = 9 \times 10^{-8} \times \left(\frac{D j_v^3 \rho_l^{0.5} \rho_v^{0.5}}{\sigma u_T}\right) \tag{14}$$

Proceedings 45th New Zealand Geothermal Workshop
15 - 17 November, 2023
Auckland, New Zealand
ISSN2703-4275

$$E_m = 1 - \frac{Re_{lc}}{Re_l} \quad (15)$$

$$h_{LM}^{+} = min\left[0.7Re_l^{0.45}, 15\right] \quad (16)$$

$$Q_{lc}\begin{cases} 0.5\pi\nu_l D(h_{LM}^{+})^2 & 0 < h_{LM}^{+} \le 5 \\ \pi\nu_l D(12.514 + 5h_{LM}^{+}\ln(h_{LM}^{+}) - 8.05h_{LM}^{+}) & 5 \le h_{LM}^{+} \le 30 \\ \pi\nu_l D(-56.09 + 2.5h_{LM}^{+}\ln(h_{LM}^{+}) + 2.74h_{LM}^{+}) & h_{LM}^{+} \ge 30 \end{cases} \quad (17)$$

$$Re_{lc} = \frac{4Q_{lc}}{D\nu_l\pi} \quad (18)$$

$$u_T = \frac{{d_d}^{1.6} g(\rho_l - \rho_v)}{13.9{\rho_v}^{0.4}{\mu_v}^{0.6}} \quad (19)$$

$$C_D\begin{cases} \frac{24}{Re_p} & Re_p < 1.92 \\ \frac{18.5}{{Re_p}^{0.6}} & 1.92 \le Re_p < 500 \\ 0.44 & Re_p \ge 500 \end{cases} \quad (20)$$

$$Re_p = \frac{u_T\rho_v d_d}{\mu_v} \quad (21)$$

$$\left(\frac{\rho_v j_v^2 d_d}{\sigma}\right)\left(\frac{d_d}{D}\right) = 0.0091 \quad (22)$$

where,

u_T	Terminal velocity (m/s)
Re_{lc}	Critical liquid film Reynolds number
h_{LM}^{+}	Modified dimensionless minimum liquid film thickness
Q_{lc}	Critical liquid film volumetric flow rate (m^3/s)
d_d	Droplet diameter (m)
g	Gravitational acceleration (m/s^2)
μ_v	Dynamic viscosity of vapour (kg/m·s)
C_D	Drag coefficient
Re_p	Droplet particle Reynolds number

2.2 Entrainment and deposition rate

The entrainment and deposition rate are assumed to be identical at the equilibrium state.

$$m_E = m_D \quad (23)$$

where,

m_E	Entrainment rate (kg/m^{2}s)
m_D	Deposition rate (kg/m^{2}s)

Kataoka et al. (2000) developed the entrainment rate from equation (4) and further developed the deposition rate by considering the concentration of droplets, which is also a function of the entrainment fraction.

$$m_E = 6.6\times10^{-7}\times\frac{\mu_l}{D}\times{Re_l}^{0.74}\times{Re_{ff}}^{0.185}\times We^{0.925}\times\left(\frac{\mu_v}{\mu_l}\right)^{0.26} \quad (24)$$

$$m_D \cong 0.022\rho_l j_l \times {Re_l}^{-0.26}\times E^{0.74}\times\left(\frac{\mu_v}{\mu_l}\right)^{0.26} \quad (25)$$

$$Re_{ff} = Re_l(1-E) \quad (26)$$

where,

Re_{ff}	Local film Reynolds number

Bae et al. (2018) improved the entrainment rate correlation of Lopez De Bertodano et al. (1997) with $k_E = 4.47\times10^{-7}$ for vertical flow to $k_E = 7.09\times10^{-7}$ which fits both vertical and horizontal flow.

$$m_E = k_E\frac{\mu_l}{D}\left[We_g\left(\frac{\Delta\rho}{\rho_v}\right)^{0.5}\left(Re_{ff} - Re_{LFC}\right)\right]^{0.925}\left[\frac{\mu_v}{\mu_l}\right]^{0.26} \quad (27)$$

$$m_D = Ck_D \quad (28)$$

$$\rho_v\frac{m_d}{m_s}k_D = k_E\frac{\mu_l}{D}\left[We_g\left(\frac{\Delta\rho}{\rho_v}\right)^{0.5}\left(Re_{ff} - Re_{LFC}\right)\right]^{0.925}\left[\frac{\mu_v}{\mu_l}\right]^{0.26} \quad (29)$$

$$We_g = \frac{\rho_v {j_v}^2 D}{\sigma} \quad (30)$$

$$C \approx \rho_v\frac{m_d}{m_s} \quad (31)$$

$$D^* = D\sqrt{\frac{\Delta\rho g}{\sigma}} \quad (32)$$

$$Fr_g = \frac{\rho_v {j_v}^2}{\Delta\rho D g} \quad (33)$$

$$\frac{k_D}{v^*} = a(Re_l)^{-0.35}(D^*)^c\left(Fr_g\right)^d \quad (34)$$

$$v^* = (0.5j_v^2 f_i)^{0.5} \quad (35)$$

$$f_i = 0.005(1 + 75\alpha_l) \quad (36)$$

where,

m_s	Steam mass flow (kg/s)
C	Droplet concentration (kg/m^3)
k_D	Droplet deposition coefficient (m/s)
We_g	Weber number
D^*	Dimensionless pipe diameter
Fr_g	Froude number
v^*	Gas friction velocity (m/s)
f_i	Interfacial friction factor
α_l	Liquid void fraction

and $Re_{LFC} = 80$ for a minimum liquid value for the liquid film Reynolds number for droplet generation.

While the values for coefficients in equation (34) are as follow:

Fr_gD	a	c	d
≤ 152.43	8.22	-0.086	-0.73
> 152.43	0.0043	1.42	0.78

In this work, the entrainment correlations outlined were applied in addition to the SPDOT model for comparison with the original GSP and SPDOT original models.

3. METHODOLOGY

The correlations presented in the previous section (2) were designed for small pipe diameters up to 10cm and are only applicable for annular flow. These correlations were developed for use in the natural gas and nuclear industry. Unfortunately, there are no entrainment correlations available in large pipe diameters. Considering that the superficial gas and liquid velocity and the liquid Reynolds number of the steam field setup by Mills & Lovelock (2020) are within the range of the correlations' experiments, the correlations are valid for use within acceptable range of error.

With the correlations mentioned in the previous section, a total of 24 model combination was created. The assumptions that were made in creating the models are:

- Entrainment happens in the separator.
- Entrainment and deposition happen simultaneously in the steam pipeline.

Proceedings 45th New Zealand Geothermal Workshop
15 - 17 November, 2023
Auckland, New Zealand
ISSN2703-4275

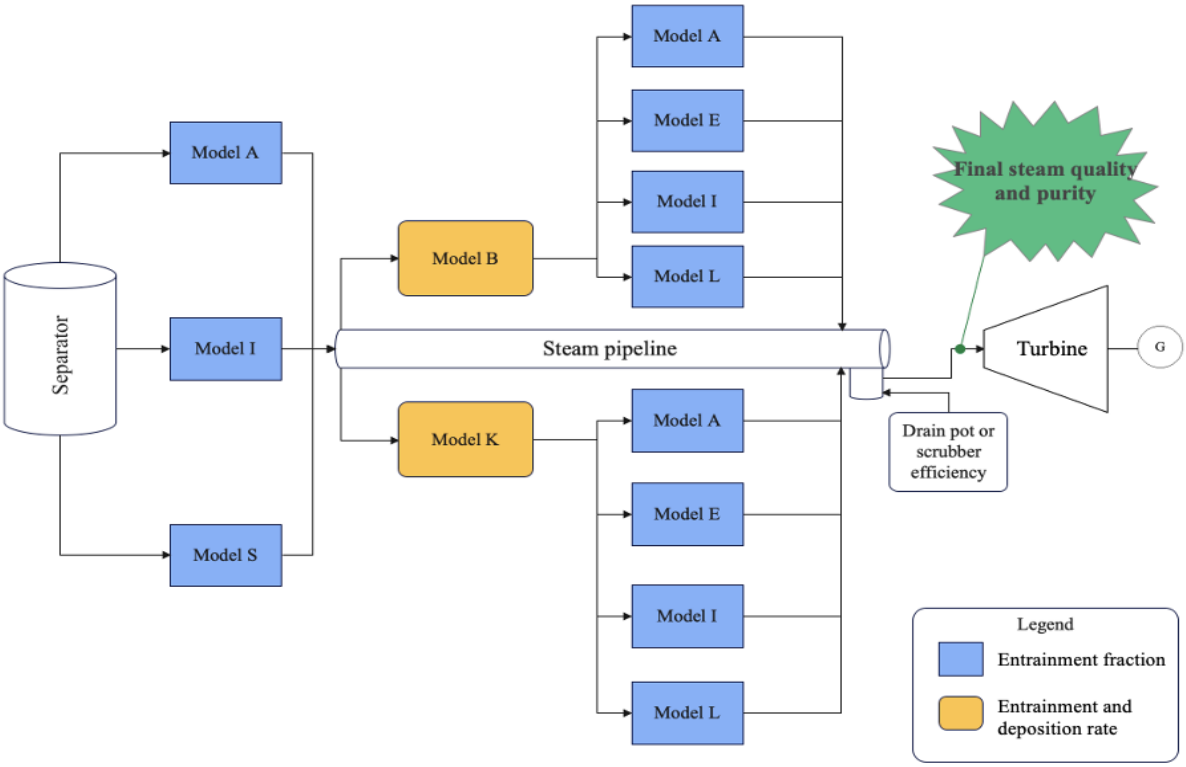

Figure 3: Entrainment model flow.

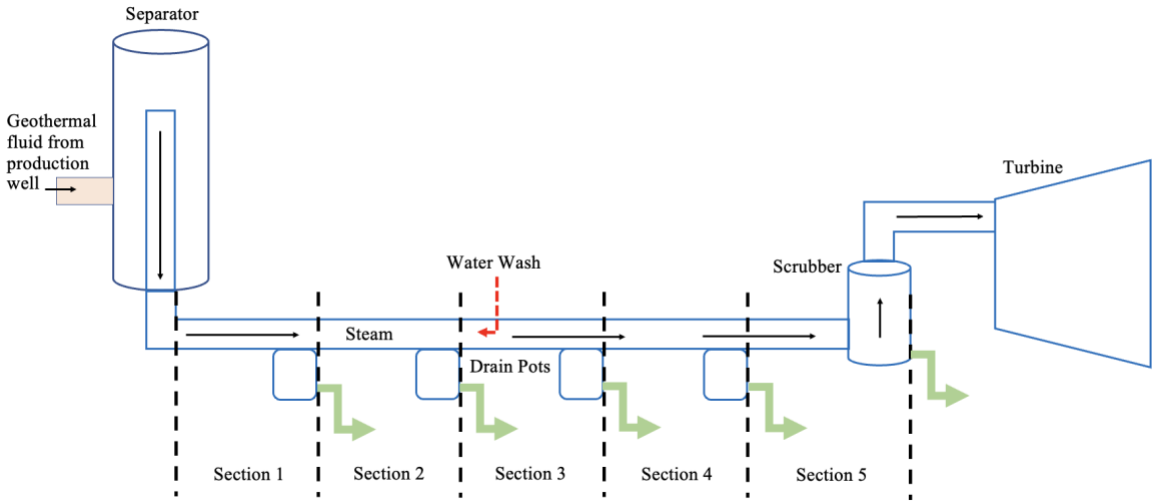

Figure 4: Steam field setup.

Table 1: Entrainment models summary.

Initial	Model	Equations
A	Al-Sarkhi et al. (2012)	(12) - (**13**)
B	Bae et al. (2018)	(27) - (36)
E	Entrainment fraction definition	(3)
I	Ishii & Mishima (1984)	(4) - (6)
K	Kataoka et al. (2000)	(24) - (26)
L	Lee et al. (2022)	(14) - (22)
S	Sawant et al. (2008)	(7) - (11)

The model names have three alphabets representing the initial of the author, from the separator to the pipeline. For example, model A_K(L) will use the Al-Sarkhi et al. (2012) entrainment fraction to calculate the droplet mass flow out of the separator. The Kataoka et al. (2000) entrainment and deposition rate to calculate the amount of newly entrained droplets and the rate of existing droplets settled to the bottom of the pipe, into the liquid film. The "L" in the bracket is the Lee et al. (2022) entrainment fraction in equation (14) is being used in the Kataoka et al. (2000) equation (**25**) and (26).

As the entrainment fraction approaches the value 1, the equation (26) becomes invalid and so does the entrainment correlation for both Model K and B. In this work, the entrainment fraction obtained by Model I in each of the pipe sections is 1. Hence model K(I) and B(I) becomes invalid. This reduces the model combinations number to 18.

Proceedings 45th New Zealand Geothermal Workshop
15-17 November, 2023
Auckland, New Zealand
ISSN 2703-4275

The entrainment models will be applied to the steam field setup in Figure 4 with parameters in Table 2, as reported in Mills & Lovelock (2020). A few assumptions from Umanzor (2022) were included, such as the outer air velocity and temperature and calcium silicate as the insulation material, which were not reported by Mills & Lovelock (2020). The results from the entrainment models will be compared to the field measurement reported by Mills & Lovelock (2020). The two models with field measurement data for comparison are the basic model (without water wash) and a water wash model in Section 3. Each section consists of a pipeline and a drain pot at the end, except for Section 5 which has a scrubber at the end of the section.

Table 2: Main parameters for steam field setup by Mills & Lovelock (2020).

Parameter name	Parameter value
Inlet fluid enthalpy	1325 kJ/kg
Inlet mass flow	500 kg/s
Inlet Chloride concentration	1500 ppm
Inlet Silica concentration	650 ppm
Separator pressure	12.5 bar
Pipeline length	250m
Pipeline diameter	1.05m
Pipeline insulation	50mm
Drain pot and scrubber spacings	50m
Drain pot efficiency	50%
Water wash flow	1% of steam flow
Water wash temperature	30°C
Assumptions by Mills & Lovelock (2020)	
Separator outlet dryness	99.95%
Scrubber efficiency	90%
Assumptions by Umanzor (2022)	
Air velocity	5 m/s
Air temperature	10°C
Insulation material	Calcium silicate
Cladding material	Aluminium
Cladding thickness	0.0009 m

4. DISCUSSION

The performance of each model is compared to the field data measured by Mills & Lovelock (2020) for the basic model (without water wash) and the water wash model. The entrainment model that has the best predictability will be used to match the actual data through calibration. The model is then used for optimisation exercise to achieve the best steam quality and purity. The aim is to achieve steam dryness of 99.95% at the turbine inlet as recommended by Morris & Mroczek (2015) and steam purity of less than 0.02 ppm Silica (for turbine inlet of less than 14 bar) and 0.002ppm Chloride as proposed by Addison & Richardson (2020).

4.1 Performance of the entrainment models

The entrainment models reduce the separator efficiency as compared to the SPDOT model up to 0.027% with the water droplets carryover, as shown in Table 3.

Table 3: Entrainment in the separator.

Model	Separator efficiency	Carryover (kg/s) Liquid film	Droplet	Total
GSP	99.950	0.0655	-	0.0655
SPDOT	99.965	0.0459	-	0.0459
Model A	99.949	0.0459	0.0215	0.0674
Model I	99.939	0.0459	0.0338	0.0797
Model S	99.938	0.0459	0.0351	0.0810

The performance of each entrainment model is compared against the field data using mean absolute error (MAE), mean absolute percentage error (MAPE), and root mean square error (RMSE). The available field data are the liquid removed from the drain pot and the concentrations of the mineral constituents in each of the drain pots. MAE measures the differences, while RMSE measures the error in the model and the data. Meanwhile, MAPE measures the accuracy of the model in forecasting the data. A lower MAPE value indicates a more accurate prediction.

$$MAE = \frac{1}{n}\sum_{i=1}^{n}|y_i - x_i| \quad (37)$$

$$MAPE = \frac{1}{n}\sum_{i=1}^{n}\left|\frac{y_i - x_i}{x_i}\right| \times 100 \quad (38)$$

$$RSME = \sqrt{\frac{1}{n}\sum_{i=1}^{n}(y_i - x_i)^2} \quad (39)$$

where,

y_i Prediction value
x_i True value
n Total number of data points

A summary of the performances of each model for each field data is presented in Table 7 to Table 9. The predicted final steam quality and purity of each model are presented in Table 10. Overall, the entrainment models predicted worse steam quality and purity entering the turbine's inlet. Model A_K(A) has the best average MAPE for liquid removed from the drain pot and will be used in the optimisation exercises.

4.2 Entrainment and deposition rate across the length

The models assume steam transport in a long straight pipeline. As the steam travels towards the power plant, the entrainment rate reduces, while the deposition rate increases slightly at Section 2 and reduces as it travels further (for most of the models), as illustrated in Figure 5 and Figure 6.

However, when water wash is introduced in early Section 3, adding water into the system increases the entrainment rate and reduces the deposition rate, as illustrated in Figure 7 and Figure 8. As the steam proceeds to the next section, the entrainment rate decreases and the deposition rate increases, as water is removed from the drain pot in the previous section. The model that predicts the highest entrainment rate in Section 3 also predicts the highest deposition rate in Section 5 but has a net entrainment rate in total.

Proceedings 45th New Zealand Geothermal Workshop
15 - 17 November, 2023
Auckland, New Zealand
ISSN2703-4275

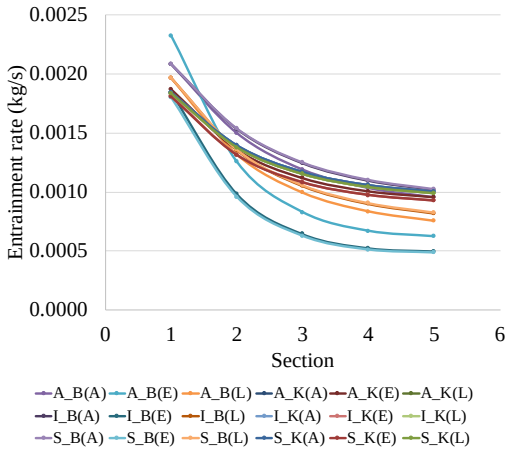

Figure 5: Entrainment rate along the pipeline (Basic model).

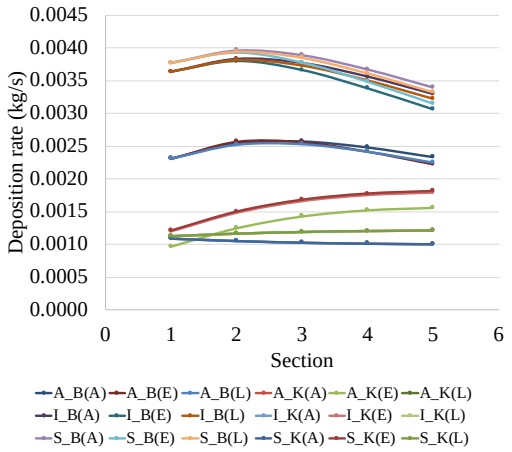

Figure 6: Deposition rate along the pipeline (Basic model).

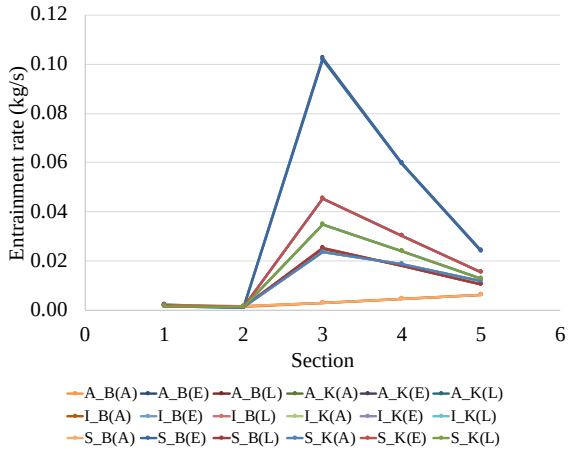

Figure 7: Entrainment rate along the pipeline (Water wash model).

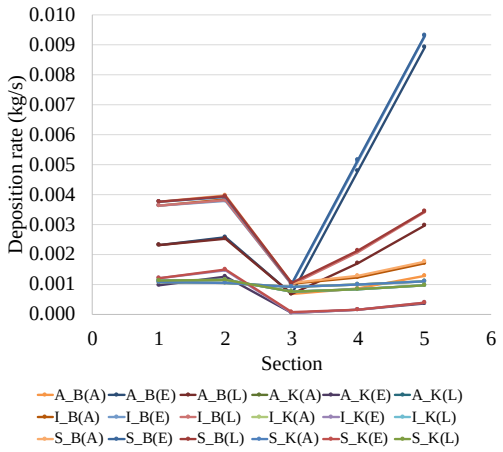

Figure 8: Deposition rate along the pipeline (Water wash model).

4.3 Pipe length optimisation

The pipe length of each section is varied from 50m to 150m to determine the effect on the steam quality and purity. The SPDOT model shows that the pressure drop and condensation rate per section length increases as the pipe length increases as shown in Table 4.

Table 4: Pipe length effect on pressure drop and condensation rate.

Pipe length (m)	Pressure drop (bar)	Condensation rate (kg/s)
50	0.0090	0.0217
75	0.0134	0.0325
100	0.0179	0.0433
125	0.0224	0.0541
150	0.0269	0.0649

Model A_K(A) predicted no significant changes in the final steam quality. The model predicted that as the pipe length increases the entrainment rate and the final steam quality increases, as illustrated in Figure 9, while the deposition rate increases slightly and remains constant.

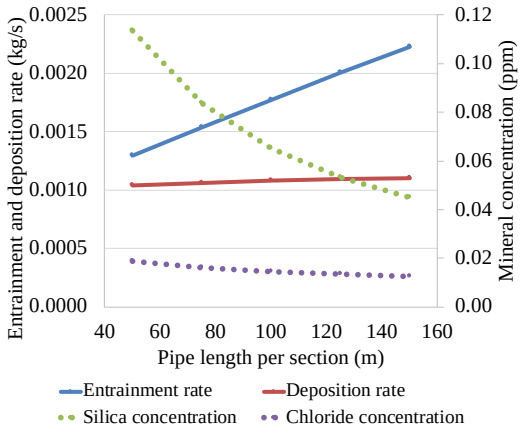

Figure 9: Pipe length effect on the entrainment and deposition rate, and final steam quality.

The total number of sections are doubled to determine the total effect on the steam quality and purity. In this case, the

Proceedings 45th New Zealand Geothermal Workshop
15 - 17 November, 2023
Auckland, New Zealand
ISSN2703-4275

scrubber is located at Section 10. The steam purity improves significantly in both the basic and water wash model, while the steam dryness remains constant in the basic model but improves a lot in the water wash model, as illustrated in Figure 10.

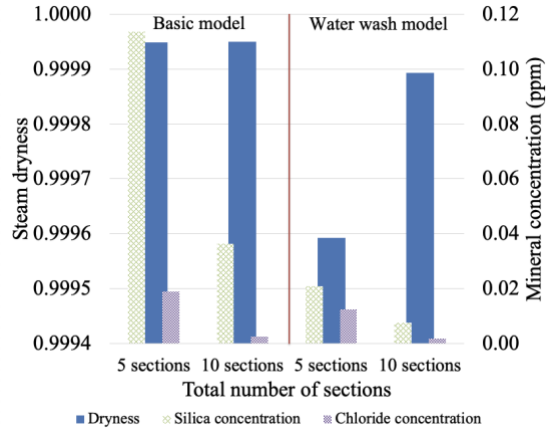

Figure 10: Double the total section number effect on the final steam quality and purity.

4.4 Pipe diameter optimisation

The pipe diameter varies from 0.8m to 1.2m to determine the effect on the steam quality and purity. The SPDOT model shows that there will be lesser pressure drop but more condensation per section length as the pipe diameter increases, as shown in Table 5.

Table 5: Pipe diameter effect on pressure drop and condensation rate.

Pipe diameter (m)	Pressure drop (bar)	Condensation rate (kg/s)
0.80	0.0351	0.0169
0.85	0.0259	0.0178
0.90	0.0194	0.0188
1.05	0.0089	0.0216
1.20	0.0046	0.0245

Model A_K(A) predicted no significant changes in the final steam quality. The model predicted that as the pipe diameter increases the entrainment rate decreases, the deposition rate increases, and the final steam quality increases as illustrated in Figure 11.

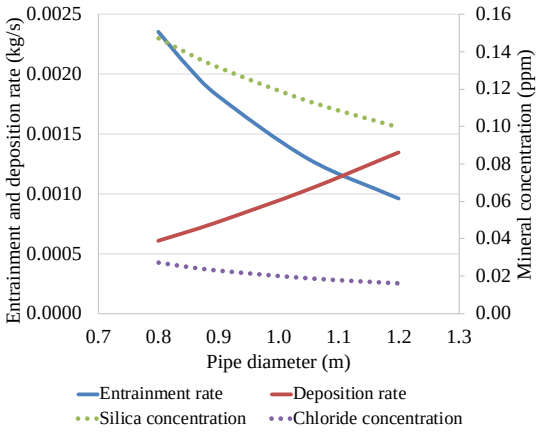

Figure 11: Pipe diameter effects on the entrainment and deposition rate, and final steam quality.

4.5 Insulation thickness optimisation

The insulation thickness of calcium silicate is varied from 0.025m to 0.125m to determine the effect on the steam quality and purity. The SPDOT model shows a decrease in condensation rate with the increasing insulation thickness, as shown in Table 6.

Table 6: Insulation thickness effect on condensation rate.

Insulation thickness (m)	Condensation rate (kg/s)
0.025	0.0383
0.050	0.0216
0.075	0.0153
0.100	0.0119
0.125	0.0098

Model A_K(A) predicted no significant changes in the final steam quality. The model predicts a decrease in the entrainment and deposition rate as the insulation thickness increases (Figure 12). Overall, the steam purity decreases as insulation thickness increases. This is mainly attributed to the decrease in condensation rate to assist in diluting the minerals to be removed via a drain pot.

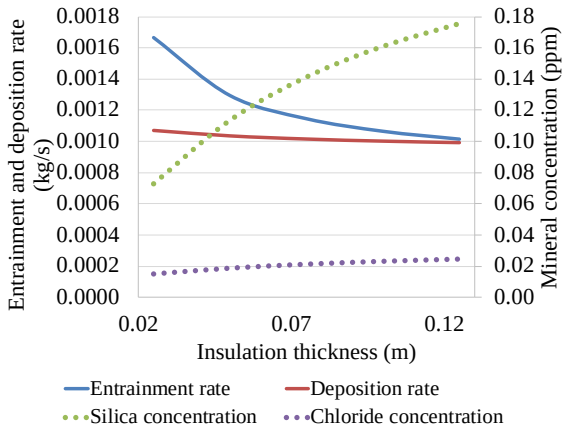

Figure 12: Insulation thickness effects on the entrainment and deposition rate, and final steam quality.

Proceedings 45th New Zealand Geothermal Workshop
15 - 17 November, 2023
Auckland, New Zealand
ISSN2703-4275

4.6 Calibrating entrainment model to match field data

All calculations in the entrainment models assumed that the system has attained an equilibrium state. This may not be accurate as the flow coming out from the separator is turbulent. This turbulent flow may cause more entrainment or deposition of water droplets which were not accounted for, but may only be done so by adding a safety factor to the equipment.

Jung (1995) recommended that the drain pot be placed at least 100 pipe diameters away from any turbulent-causing fittings, including elbows or a drain pot, for optimum performance. The field data in Figure 13 signifies that the flow in the system has not achieved an equilibrium state. The reduction of liquid removed in the drain pot in Section 3 and 4 suggests a disturbance in the flow or more entrainment in those sections. This can be proven if the water washing equipment is in Section 3 during the measurement.

On the other hand, the assumed efficiency of the scrubber in Section 5 of 90% efficiency by Mills & Lovelock (2020) is too optimistic. All the models (GSP, SPDOT and entrainment models) have the highest error in predicting the liquid removed in the scrubber in Section 5. The entrainment models predicted quite closely to the field data from Sections 1 to 4 but have the worst prediction in Section 5 (as compared to the GSP and SPDOT models). The high error in Section 5 increases the overall error of each model in Table 7 toTable 9. This over-prediction is due to the removal of 90% of the water droplets in the system on top of the removal of 90% of the water from the system via the scrubber.

A safety factor of insulation can be added to increase the condensation rate. Insulation is not always 100% efficient, especially at bends and at joints that are not sealed properly or air gaps in between the layers of pipe and insulation and cladding.

The entrainment model predicts the liquid removal more closely to the field data than GSP and SPDOT models for both the basic and water wash models (except for Section 5). This shows that the distinguishment between the liquid flowing at the bottom of the pipe for removal by drain pot and the water droplets flowing in the gas core is not removed has a significant impact on the model. Model A_K(A) calibrated matches the field data for the basic model as shown in Figure 13, with MAPE of 0.58%.

However, Model A_K(A) calibrated does not match the water wash model field data. The model underpredicts the liquid removal in Sections 3 and 5, as shown in Figure 14.

Another calibration is performed, and the Model A_K(A) recalibrated matches the field data with MAPE of 0.31%. Water washing is the introduction of water spraying into the system to capture the volatile minerals in the steam and removed them via a drain pot. The act of water spraying many droplets into the system and the interaction of these droplets with the existing water droplets in the system is complicated and has not been considered. The recalibration exercise infers that the turbulence in Section 3 that reduces the drain pot efficiency in the basic model helps mix the water droplets more effectively and deposits faster into the water film at the bottom of the pipeline for removal. The type of scrubber used in Section 5 is not known, but the recalibration exercise infers that the scrubber efficiency is affected by the wetness of the incoming steam. The efficiency increases as the wetness of the incoming steam is higher.

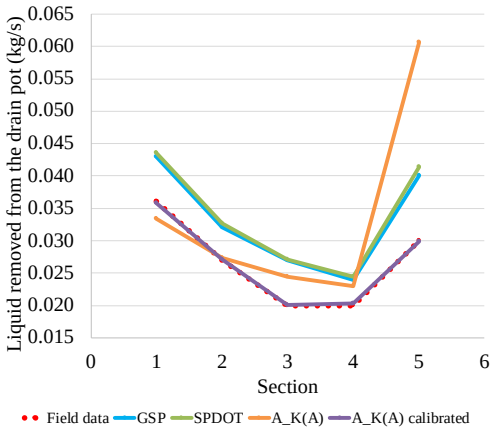

Figure 13: Liquid removed from the drain pot field data against GSP, SPDOT and A_K(A) for the Basic model.

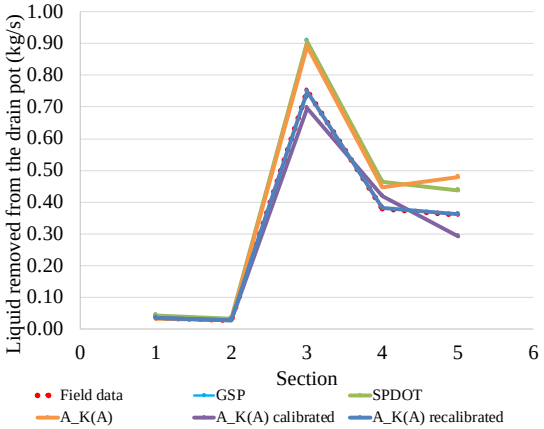

Figure 14: Liquid removed from the drain pot field data against GSP, SPDOT and A_K(A) for the Water wash model.

4.7 Water wash optimisation

The location of the water wash in the steam field affects the steam's dryness and purity. Water washing improves the steam's purity by capturing the volatile minerals in the steam phase, but reduces the steam's dryness (slightly).

The SPDOT model predicted that washing at Section 3 gives the best outcome while achieving the desired steam dryness and Silica concentration (Figure 15). A drain pot must be replaced with a higher efficiency of 85% to lower the Chloride concentration to below 0.002ppm.

Figure 16 shows that Model A_K(A) predicted that washing at each section affects the steam purity differently than what was predicted by the SPDOT model. The concentration of Chloride in the steam entering the turbine is the least when washing in Section 1, as opposed to the constant concentration predicted by SPDOT. This shows the effect of entrainment and deposition on the steam purity. Washing upstream is desirable as it achieves the highest steam dryness and purity. Washing upstream should be desirable as most of the Silica concentration was removed early in the system and poses less possibility of deposition on the equipment

Proceedings 45th New Zealand Geothermal Workshop
15 - 17 November, 2023
Auckland, New Zealand
ISSN2703-4275

downstream. In this case, replacing all the drain pots to 85% efficiency must be done to achieve the minimum requirements of steam purity.

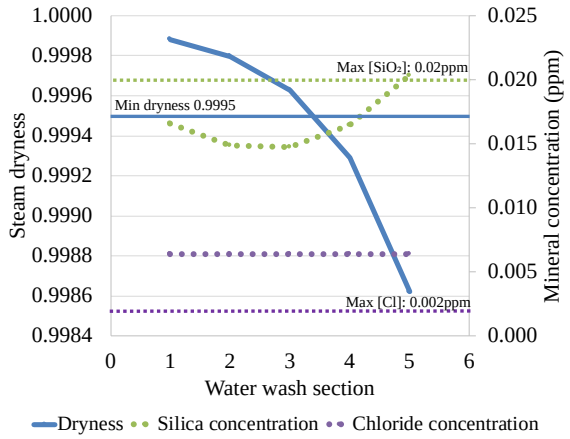

Figure 15: Water wash location effect on the final steam quality and purity (SPDOT model).

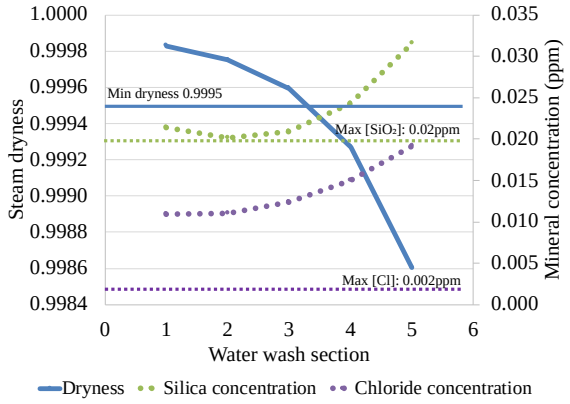

Figure 16: Water wash location effect on the final steam quality and purity (Model A_K(A)).

However, when Model A_K(A) recalibrated is used for the optimisation exercise, replacing all the drain pots and the scrubber with the highest 95% efficiency is still insufficient to achieve the desired steam purity. A few of the options to achieve the steam purity, in this case, is to reduce the insulation thickness or increase the water wash flow rate. These options are not ideal as they reduce the steam flow rate and reduce the overall power generation.

4.8 Optimisation exercises conclusion

Designing the steam field is the essence of the power plant's performance of smooth production. The calibration and water wash optimisation exercises signify that the scrubbing line's equipment were underutilised. Upgrading or retrofitting higher efficiency equipment into the setup only helps improve the steam purity slightly and is costly. The best solution is to have a steam field setup long enough to have the equipment working at their designed efficiency as recommended by Jung (1995) and Zarrouk & Purnanto (2015).

5. CONCLUSION

A close-to-perfect steam purity modelling has yet to be established for the geothermal industry. The lack of CFD study on water droplets tracking and establishment of entrainment correlation in large diameter pipe make it difficult to accurately model the steam purity. This work presents a stepping stone in developing a model to better understand the entrainment in the steam pipeline.

The optimisation exercises provided an understanding of the equipment features to the entrainment and deposition rate.

- The entrainment rate decreases while the deposition rate remains almost constant as the steam flows.
- Increasing pipe diameter leads to a decrease in entrainment rate but an increase in deposition rate.
- Increasing insulation thickness decreases the entrainment rate with an almost constant deposition rate.
- Increasing pipe diameter and reducing insulation thickness increases steam purity.
- Water wash introduces a net entrainment rate to the system.
- Water wash helps capture volatile minerals in the steam and remove them via a drain pot.
- Water wash upstream dilutes and removes more Silica from the system.

In summary, the entrainment models have better predictability than the GSP and SPDOT models. They predicted worse steam quality and purity entering the turbine's inlet. Some solutions were recommended to help improve the steam quality and purity using Model A_K(A) recalibrated, which was matched to the field data. However, an over-efficient scrubbing line will be a waste of resources and investment.

The models assumed that the system has attained equilibrium and the steam flows in a long straight pipeline. We are working on improving the model to include pipe fittings, bends, and equipment in the pipeline (which will cause turbulence to the system). Case studies will be done using field data to verify further the model's application to the actual geothermal steam field.

REFERENCES

Addison, D., & Richardson, I. (2020). GEOTHERMAL STEAM TURBINE DEPOSITION FUNDAMENTALS AND PROPOSED IAPWS GEOTHERMAL STEAM PURITY LIMITS. *42nd New Zealand Geothermal Workshop*.

Al-Sarkhi, A., Sarica, C., & Qureshi, B. (2012). Modeling of droplet entrainment in co-current annular two-phase flow: A new approach. *International Journal of Multiphase Flow*, *39*, 21–28.

Bae, B., Kim, T., Jeong, J., Kim, K., & Yun, B. (2018). Droplet entrainment and deposition rates in a horizontal annular flow for SPACE code. *Progress in Nuclear Energy*, *109*, 45–52.

Bangma, P. (1961). *THE DEVELOPMENT AND PERFORMANCE OF A STEAM-WATER SEPARATOR FOR USE ON GEOTHERMAL BORES*.

Ishii, M., & Grolmes, M. A. (1975). Inception criteria for droplet entrainment in two-phase concurrent film flow. *AIChE Journal*, *21*(2), 308–318.

Ishii, M., & Mishima, K. (1984). TWO-FLUID MODEL AND HYDRODYNAMIC CONSTITUTIVE RELATIONS. *Nuclear Engineering and Design*, *82*, 107–126.

ISSN2703-4275

Jung, D. B. (1995). Drip-pot Applications. In *Geothermal Resources Council TRANSACTIONS* (Vol. 19).

Kataoka, I., Ishii, M., & Nakayama, A. (2000). Entrainment and desposition rates of droplets in annular two-phase flow. *International Journal of Heat and Mass Transfer*, *43*, 1573–1589.

Lazalde-Crabtree, H. (1984). *Design Approach of Steam-Water Separators and Steam Dryers For Geothermal Applications*.

Lee, J., Skorek, T., Junk, M., & Schöffel, P. J. (2022). Improved correlation of liquid entrainment fraction in horizontal pipes. *Nuclear Engineering and Design*, *388*.

Lopez De Bertodano, M. A., Jan, C.-S., & Beus, S. G. (1997). Annular flow entrainment rate experiment in a small vertical pipe. In *Nuclear Engineering and Design*, *178*, 61-70.

Mantilla, I. (2008). *MECHANISTIC MODELING OF LIQUID ENTRAINMENT IN GAS IN HORIZONTAL PIPES* [Doctor of Philosophy]. The University of Tusla.

Mills, T. D., & Lovelock, B. G. (2020). *GEOTHERMAL STEAM PURITY MODELLING-THEORY AND PRACTICE*. *42nd New Zealand Geothermal Workshop*.

Morris, C. J., Mroczek, E. K., & Misa, T. N. (2019). Geothermal steam condition performance monitoring. *Geothermics*, *81*, 101–112.

Morris, C., & Mroczek, E. (2015). *TURBINE SCALING*. *36th New Zealand Geothermal Workshop*.

Pan, L., & Hanratty, T. J. (2002). Correlation of entrainment for annular flow in horizontal pipes. *International Journal of Multiphase Flow*, *28*, 385–408.

Pointon, A. R., Mills, T. D., Seil, G. J., & Zhang, Q. (2009). Computational Fluid Dynamic Techniques for Validating Geothermal Separator Sizing. *GRC Transactions*, *33*, 943–948.

Richardson, I., Addison, S., & Thompson, G. (2013). STEAM PURITY CONSIDERATIONS IN GEOTHERMAL POWER GENERATION. In *35 th New Zealand Geothermal Workshop*.

Sawant, P., Ishii, M., & Mori, M. (2008). Droplet entrainment correlation in vertical upward co-current annular two-phase flow. *Nuclear Engineering and Design*, *238*(6), 1342–1352.

Umanzor, C. (2022). *Optimization of Moisture Removal System in Geothermal Steamfields* [Master of Engineering]. University of Auckland.

Umanzor, C., & Zarrouk, S. J. (2022). *The Steamfield Process Design and Optimisation Tool (SPDOT)*.

Van Rossum, J. J. (1959). Experimental investigation of horizontal liquid films Wave formation, atomization, film thickness. In *Chemical Engineering Science*, *11*, 35-52.

Zarrouk, S. J., & Purnanto, M. H. (2015). Geothermal steam-water separators: Design overview. In *Geothermics*, *53*, 236–254.

Table 7: Absolute and relative error of entrainment models against measured data of liquid removed from the drain pot.

	Basic model			Water wash model		
Model	MAE	MAPE	RSME	MAE	MAPE	RSME
GSP	0.0066	25.26	0.0069	0.0658	20.42	0.0867
SPDOT	0.0072	27.53	0.0076	0.0656	21.16	0.0860
A_B(A)	0.0081	30.20	0.0126	0.0664	15.77	0.0881
A_B(E)	0.0082	30.54	0.0124	0.0644	16.92	0.0962
A_B(L)	0.0081	30.26	0.0124	0.0659	16.03	0.0874
A_K(A)	0.0082	29.60	0.0140	0.0661	15.63	0.0879
A_K(E)	0.0083	29.97	0.0137	0.0657	15.96	0.0889
A_K(L)	0.0082	29.70	0.0138	0.0659	15.79	0.0881
I_B(A)	0.0101	37.80	0.0161	0.0684	16.63	0.0904
I_B(E)	0.0101	38.03	0.0157	0.0664	17.79	0.0994
I_B(L)	0.0101	37.86	0.0159	0.0679	16.89	0.0901
I_K(A)	0.0104	37.00	0.0189	0.0683	16.25	0.0910
I_K(E)	0.0104	37.43	0.0183	0.0678	16.63	0.0923
I_K(L)	0.0104	37.10	0.0187	0.0681	16.40	0.0914
S_B(A)	0.0103	38.60	0.0165	0.0686	16.72	0.0906
S_B(E)	0.0103	38.81	0.0160	0.0666	17.89	0.0998
S_B(L)	0.0103	38.65	0.0163	0.0681	16.98	0.0903
S_K(A)	0.0107	37.77	0.0194	0.0685	16.31	0.0913
S_K(E)	0.0107	38.20	0.0188	0.0681	16.70	0.0927
S_K(L)	0.0107	37.87	0.0192	0.0683	16.47	0.0918
Calibration exercise (Section 4.6)						
A_K(A) - calibrated	0.0001	0.58	0.0002	0.0322	7.42	0.0423
A_K(A)- recalibrated				0.0006	0.31	0.0007

Table 8: Absolute and relative error of entrainment models against measured data of Chloride concentration in liquid removed from the drain pot.

	Basic model	Water wash model

ISSN2703-4275

Model	MAE	MAPE	RSME	MAE	MAPE	RSME
GSP	155	17.15	185	109	16.88	172
SPDOT	166	18.76	196	116	22.64	180
A_B(A)	132	17.50	170	100	16.70	162
A_B(E)	130	16.81	167	101	24.18	161
A_B(L)	132	16.99	171	102	17.95	164
A_K(A)	144	24.08	170	91	22.24	149
A_K(E)	138	22.48	166	91	24.05	148
A_K(L)	141	23.25	169	92	22.82	150
I_B(A)	150	27.64	168	83	35.83	134
I_B(E)	144	25.48	164	87	43.97	137
I_B(L)	148	26.88	167	84	37.51	135
I_K(A)	187	42.21	207	65	47.14	112
I_K(E)	177	38.87	195	68	48.48	114
I_K(L)	185	41.35	204	66	47.97	113
S_B(A)	153	28.72	170	81	37.87	132
S_B(E)	147	26.45	165	86	46.09	135
S_B(L)	151	27.96	168	83	39.60	133
S_K(A)	191	43.98	214	63	49.83	110
S_K(E)	181	40.50	201	66	51.13	111
S_K(L)	189	43.12	211	64	50.69	110
Calibration exercise (Section 4.6)						
A_K(A) - calibrated	173	28.54	212	116	25.01	189

Table 9: Absolute and relative error of entrainment models against measured data of Silica concentration in liquid removed from the drain pot.

	Basic model			Water wash model		
Model	MAE	MAPE	RSME	MAE	MAPE	RSME
GSP	95	17.17	102	56	17.05	86
SPDOT	74	12.41	85	48	8.92	76
A_B(A)	59	8.83	76	48	16.46	73
A_B(E)	59	8.79	76	49	23.63	73
A_B(L)	60	8.91	77	49	17.82	74
A_K(A)	56	9.36	71	45	20.33	68
A_K(E)	55	8.83	71	46	22.06	68
A_K(L)	56	9.15	71	46	20.98	69
I_B(A)	55	8.77	71	47	25.52	69
I_B(E)	54	8.34	72	50	32.80	71
I_B(L)	55	8.61	72	48	27.08	70
I_K(A)	59	11.97	70	42	32.26	60
I_K(E)	56	10.86	68	43	33.68	60
I_K(L)	58	11.64	70	42	33.03	60
S_B(A)	55	8.87	71	47	26.47	69
S_B(E)	54	8.41	72	50	33.76	70
S_B(L)	55	8.72	71	48	28.05	69
S_K(A)	61	12.43	71	41	33.51	59
S_K(E)	56	11.08	68	42	34.91	60
S_K(L)	59	12.10	70	42	34.30	59
Calibration exercise (Section 4.6)						
A_K(A) - calibrated	68	11.16	87	54	21.57	83

Table 10: Final steam purity and quality by entrainment models.

	Basic model		Water wash model	
Model	Steam dryness	Steam quality, TDS (ppm)	Steam dryness	Steam quality, TDS (ppm)
GSP	1.0000	0.0770	0.9996	0.0220

Proceedings 45th New Zealand Geothermal Workshop
15 - 17 November, 2023
Auckland, New Zealand
ISSN2703-4275

SPDOT	1.0000	0.0946	0.9996	0.0211
A_B(A)	1.0000	0.1191	0.9996	0.0296
A_B(E)	1.0000	0.1176	0.9995	0.0385
A_B(L)	1.0000	0.1177	0.9996	0.0313
A_K(A)	0.9999	0.1323	0.9996	0.0332
A_K(E)	0.9999	0.1294	0.9996	0.0354
A_K(L)	0.9999	0.1309	0.9996	0.0341
I_B(A)	0.9999	0.1334	0.9996	0.0357
I_B(E)	0.9999	0.1296	0.9995	0.0457
I_B(L)	0.9999	0.1320	0.9996	0.0379
I_K(A)	0.9999	0.1597	0.9996	0.0419
I_K(E)	0.9999	0.1535	0.9996	0.0442
I_K(L)	0.9999	0.1581	0.9996	0.0430
S_B(A)	0.9999	0.1349	0.9996	0.0364
S_B(E)	0.9999	0.1309	0.9995	0.0465
S_B(L)	0.9999	0.1335	0.9996	0.0386
S_K(A)	0.9999	0.1626	0.9996	0.0428
S_K(E)	0.9999	0.1561	0.9996	0.0451
S_K(L)	0.9999	0.1610	0.9996	0.0440
Calibration exercise (Section 4.6)				
A_K(A) - calibrated	0.9996	0.3582	0.9971	0.1853

Table 11: Original GSP and SPDOT models, and calibrated entrainment model data against field data.

	Model	Section 1	Section 2	Section 3	Section 4	Section 5
	Liquid removed from the drain pot (kg/s)					
	Field data	0.0360	0.0270	0.0200	0.0200	0.0300
	GSP	0.0430	0.0320	0.0270	0.0240	0.0400
	SPDOT	0.0436	0.0326	0.0271	0.0244	0.0414
	A_K(A) calibrated	0.0358	0.0271	0.0200	0.0203	0.0299
	Chloride concentration in liquid removed from the drain pot (ppm)					
	Field data	1858	1251	757	423	224
Basic model	GSP	1539	1036	627	350	186
	SPDOT	1527	1020	613	341	181
	A_K(A) calibrated	1472	1077	766	549	397
	Silica concentration in liquid removed from the drain pot (ppm)					
	Field data	877	688	520	385	281
	GSP	726	569	431	319	233
	SPDOT	739	588	454	344	258
	A_K(A) calibrated	719	592	481	393	321
	Liquid removed from the drain pot (kg/s)					
	Field data	0.0360	0.0270	0.7500	0.3800	0.3600
	GSP	0.0430	0.0320	0.9070	0.4640	0.4360
	SPDOT	0.0436	0.0326	0.9051	0.4634	0.4365
	A_K(A) calibrated	0.0358	0.0271	0.6960	0.4197	0.2932
	A_K(A) recalibrated	0.0358	0.0271	0.7495	0.3812	0.3609
	Chloride concentration in liquid removed from the drain pot (ppm)					
Water wash model	Field data	1858	1251	25	24	23
	GSP	1539	1036	21	20	19
	SPDOT	1527	1020	18	18	17
	A_K(A) recalibrated	1472	1077	31	31	31
	Silica concentration in liquid removed from the drain pot (ppm)					
	Field data	877	688	24	24	23
	GSP	726	569	20	20	19
	SPDOT	739	588	23	23	22
	A_K(A) recalibrated	719	592	30	30	29

ISSN2703-4275